Journal of Materials Chemistry A

Accepted Manuscript

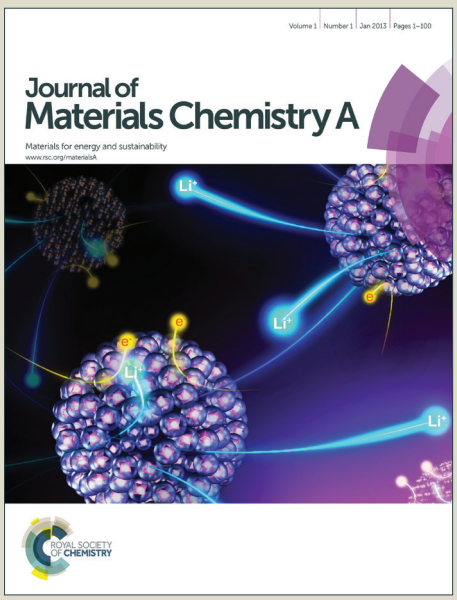

ROYAL SOCIETY OF CHEMISTRY

www.rsc.org/materialsA

Journal Name

ARTICLE

Pyridomethene-BF_2 complex/phenothiazine-hybrid sensitizer with high molar extinction coefficient for efficient sensitized solar cells

Received 00th January 20xx,
Accepted 00th January 20xx

DOI: 10.1039/x0xx00000x

www.rsc.org/

Yan-Duo Lin,[a] Bo-Yu Ke,[b] Yuan Jay Chang,[c] Po-Ting Chou,[a] Kang-Ling Liau,[d] Ching-Yang Liu[b] and Tahsin J. Chow*[a]

A series of new pyridomethene-BF_2/phenothiazine-hybrid metal-free organic sensitizers **K1**-**K8** containing different π-spacers were synthesized and applied in dye-sensitized solar cells (DSSC). The introduction of the pyridomethene-BF_2 complex unit to the phenothiazine chromophore displayed a high molar extinction coefficient in favor of light-harvesting. Quantum chemical calculations were performed by using the density functional theory (DFT) at the B3LYP/6-31G (d,p) level to investigate the structural properties and electron density distributions of these dyes. The effect of dyes **K1**-**K8** on the performance of DSSC was investigated systematically with comparisons to the plane phenothiazine dyes **R1** and **R2**. Upon co-adsorption with deoxycholic acid, the dye **K3** with a thiophene unit between the phenothiazine and pyridomethene-BF_2 units exhibited the best photovoltaic performance. The short-circuit current density (J_{sc}) was 15.43 mA cm^{-2} with an open-circuit voltage (V_{oc}) 0.69 V and a fill factor (FF) 0.62, that corresponded to a power-conversion efficiency (η) 6.58% under AM 1.5G irradiation (100 mW · cm^{-2}) condition. The *n*-hexyl chain attached to the thiophene in **K4**-**K5** exhibitted an effect of improving the V_{oc} value. The presence of the phenyl pyridomethene-BF_2 moiety at the *N*(10) atom of phenothiazine in **K6**-**K8** showed a good effect of reducing π-π aggregation. These results revealed the advantage of incorporating a pyridomethene-BF_2 group in the dyes for high performance DSSC cells.

Introduction

Dye-sensitized solar cells (DSSC) have been intensively studied as promising photovoltaic device since its discovery by O'Regan and Grätzel et al. in 1991.[1] This type of solar cell has an advantage of low-cost in fabrication comparing to the classical silicon-based solar cells. The dye sensitizer plays a crucial factor in the performance of DSSC, both on power conversion efficiency (η) as well as on device stability. In the development of DSSC, metal complexes such as **N3**,[2] **N719**,[3] black dye[4] and **YD2-*o*-C8**[5] have exhibited impressive solar energy-to-electricity conversion efficiencies exceeding 10% under illumination of standard global air mass 1.5 (AM1.5G). In contrast to metal complexes, organic dyes have been extensively explored in recent years due to their low cost, environmental friendliness, high molar absorption coefficient, tunable spectra, and others. Various kinds of organic dyes based on coumarin,[6] phenothiazine,[7-10] cyanine,[11] indoline,[12] triphenylamine,[13-20] derivatives have been shown to work effectively for DSSC.

Although a remarkable progress has been made, further optimization of the chemical structures of organic dyes is still in need. One of the main shortcomings of metal complex dyes is their weak absorption in the red region of visible spectrum. The molar extinction coefficient of sensitizers in the visible region is an important factor that affects the DSSC efficiency. A high absorption coefficient in the visible wavelength will increase the value of short-circuit current density (J_{sc}). Among various strategies for increasing molar extinction coefficient, one common tactic is to make the π-chromophore more rigid, in order to suppress the rotational disorder of molecules, and to enhance the delocalization capacity of π-electrons. However, rod-like molecules may magnify aggregate formation between molecules and facilitate the recombination of electrons with triiodide electrolyte.[21] The incorporation of an additional electron donor unit on the sensitizer to form starburst 2D–π–A configuration is another approach to enhance the molar extinction coefficient.[22-24] In either of these two strategies, the complicated synthetic pathways usually become the limiting factor on practical applications. Therefore it is necessary to design relatively small and simple organic compounds to minimize the difficulty of synthesis.

Organoboron complexes are highly attractive dyes of high photochemical stability. They exhibit high molar absorptivity and electron-accepting property. Among various organoboron complexes, boron dipyrromethene derivatives (BODIPY)[25] have been widely employed as biomolecule labeling dyes,[26] chemosensors,[27] and photodynamic therapy.[28] By virtue of their high absorptivity in the visible and near-IR regions, BODIPY dyes have been used previously in both liquid electrolyte and solid state DSSC. However, the overall

[a] *Institute of Chemistry, Academia Sinica, Taipei 115, Taiwan.E-mail: chowtj@gate.sinica.edu.tw*
[b] *Department of Applied Chemistry, Chinese Culture University, Taipei 111, Taiwan*
[c] *Department of Chemistry, Tung Hai University, Taichung 407, Taiwan.*
[d] *Department of Chemistry, National Central University, Chung-Li 320, Taiwan.*
† Electronic Supplementary Information (ESI) available: Synthetic procedures, Scheme S1-4, Fig. S1-8 and Table S1-2. See DOI: 10.1039/x0xx00000x

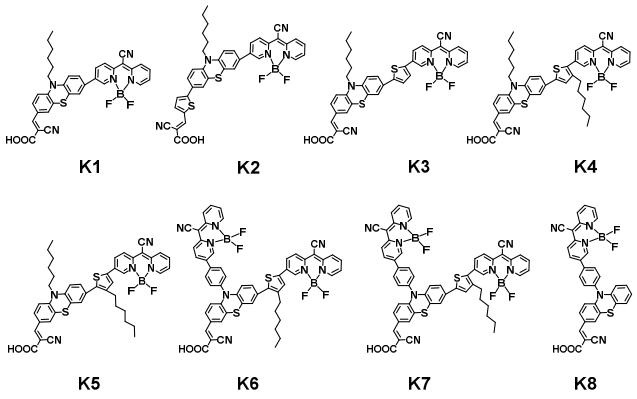

Fig. 1 Molecular structures of dyes **K1–K8** containing pyridomethene-BF_2 complex as additional donor.

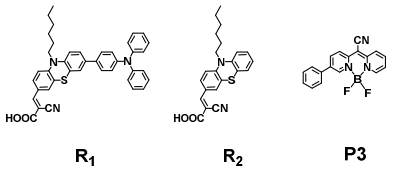

Fig. 2 Molecular structures of reference dyes **R1** and **R2** and the parent pyridomethene-BF_2 complex **P3**.

conversion efficiencies were not quite satifactory.[29-44] In our earlier report, we have designed a different pyridomethene-BF_2 complex, with a similar structure to BODIPY, that exhibited a very large extinction coefficient ($\varepsilon>5\times10^4$ M^{-1} cm^{-1}).[45] With this experience, we envisioned that the introduction of the pyridomethene-BF_2 complex unit into the framework of a sensitizer will be beneficial to light-harvesting. To the best of our knowledge, there is no report that uses pyridomethene-BF_2 complexes as a sensitizer dye on DSSC up to date.

Unlike BODIPY, phenothiazine-based sensitizers have been successfully utilized in DSSC and exhibited high conversion efficiency.[8,10] The structure of phenothiazine contains an electron-rich heterocycle made with sulfur and nitrogen. Its geometry is not planar in the group state, but tilts slightly like a butterfly. Therefore it is not a fully π–conjugate system in a classical sense across the three rings of phenothiazine, which leads to a small oscillator strength (*f*) and a weak intramolecular charge transfer (ICT) efficiency. It is expected that grafting a pyridomethene-BF_2 unit on a phenothiazine backbone may increase the molar absorptivity as a whole.

We designed and synthesized a series of dyes **K1–K8** by incorporating phenothiazine and pyridomethene-BF_2 into one chromophore (Fig. 1). In the structure of compound **K1**, a pyridomethene-BF_2 complex unit is linked to the C(7) position of phenothiazine and a cyanoacrylic acid moiety to the C(3) position. An alkyl side chain is attached to the phenothiazine nitrogen atom in order to increase the solubility and to reduce the dark current by covering the surface of TiO_2 from exposing to the electrolyte.[46-48] In compounds **K2** and **K3**, a thiophenylene group was introduced to the main chain of the dyes to broaden the absorption wavelength range. In compounds **K4** and **K5**, an additional *n*-hexyl chain was attached to the thiophene unit to further improve the surface morphology. In compounds **K6** and **K7**, a second pyridomethene-BF_2 moiety was attached to the phenothiazine nitrogen atom, not only to enhance the molar extinction coefficient ($\varepsilon>1\times10^5$ M^{-1} cm^{-1}), but also to function as insulator to suppress intermolecular π-π stacking. To clarify the influence of the second pyridomethene-BF_2 unit on **K6** and **K7**, compound **K8** was prepared to serve as a reference material. Another three reference compounds **R1**, **R2**[7] and **P3** (Fig. 2) were also prepared to clarify the functions of both phenothiazine and pyridomethene-BF_2 moieties in **K1**-**K8**. In compound **R1**, a triphenylamine group replaces the pyridomethene-BF_2 unit in **K1** as an electron-donating group. Compounds **R2** and **P3** provided the simplest models for expressing the properties of phenothiazine and pyridomethene-BF_2, respectively. It is known that organoboron complexes possess high photochemical stability, therefore the stability of all the pyridomethene-BF_2 containing dyes are also examined. Detailed structural and electronic properties were carried out by using density function theory (DFT) and time-dependent DFT (TDDFT) at the B3LYP/6-31G (d,p) level for all molecules. The synthetic details for the preparations of dyes **K1-K8**, **R1** and **P3** are described in the ESI.

Results and discussion

Photophysical properties

The UV-vis absorption spectra of **K** and **R** series dyes in THF solution are shown in Fig. 3. The absorption peaks as well as their molar extinction coefficients are listed in Table 1. All dyes displayed two major absorption maxima: *i.e.*, a short wavelength one at around 300-350 nm corresponds to the π-π* transition and a long wavelength one at about 440-480 nm. The featureless long absorption bands of **R1** and **R2** are assigned to an intramolecular charge transfer (ICT) transition. In contrast, the long wavelength absorption bands of all **K** dyes show a shoulder on the blue edge. This absorption feature is apparently different from that of **R** dyes. In addition, the longer wavelength absorption bands of **K** dyes blue shifted with increasing solvent polarity (*e.g.*, **K1** from 466 nm in THF to 460 nm in MeCN, Fig. S1). When compared to the reference dye **R1** with a triphenylamine group, the replacement of a pyridomethene-BF_2 unit in **K1** red-shifts the long absorption peak from 450 nm (**R1**) to 466 nm (**K1**) (Table 1), and increases the molar extinction coefficient from 1.64×10^4 M^{-1} cm^{-1} (**R1**) to 4.63×10^4 M^{-1} cm^{-1} (**K1**). The absorption band of **K2** is nearly the same as that of **K1**, except that the absorption band is wider and the molar extinction coefficient is higher (5.74×10^4 M^{-1} cm^{-1} for **K2**) due to the presence of a thiophene unit. The spectrum of **K3** shows a distinct red-shift of 15 nm with respect to that of **K1**, which is caused by an increase in the π-conjugation length. The molar extinction coefficient of **K3** was further enhanced to 8.61×10^4 M^{-1} cm^{-1} that ensures a good

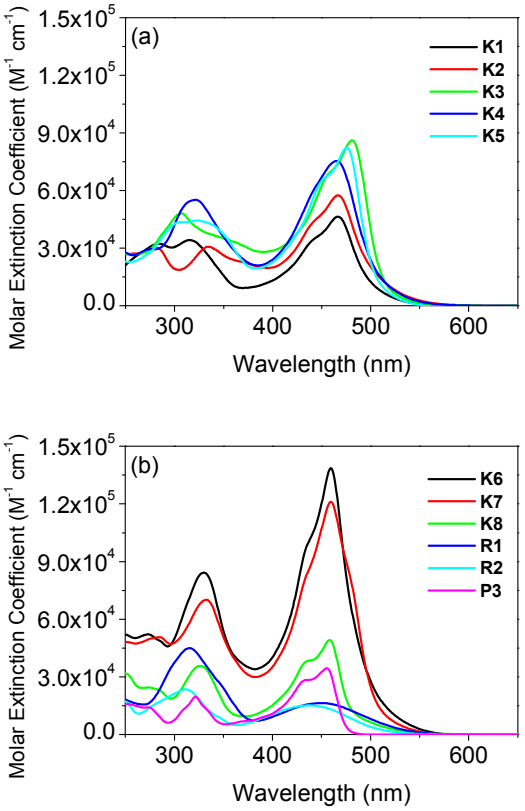

Fig. 3 Absorption spectra of **K**, **R**, and **P3** dyes in the THF.

light-harvesting ability in DSSC. The long wavelength absorption bands of **K4** and **K5** are blue-shifted by 16 and 6 nm with respect to **K3**. The presence of a hexyl substituent on the thiophene disturbs the planar geometry, therefore reduced the degree of π-conjugation. The geometry change was evidenced by molecular modelling analysis according to the density function theory (DFT) with B3LYP functional in combination with the standard 6-31G (d,p) basis set. The optimized geometry of **K3** revealed that the two dihedral angles between the thiophene unit and its adjacent groups are 24.33° and 25.55° (Fig. 4). The corresponding dihedral angles in **K4** and **K5**, however, increased to 40.89° and 43.28°. As a result, the spectrum of **K3** displayed not only a red-shift to those of **K4** and **K5**, but also a higher molar extinction coefficient. In the spectra of **K6** and **K7**, a very large molar extinction coefficient of 1.39×10^5 and 1.21×10^5 $M^{-1}cm^{-1}$ at 460 nm were observed, as a result of the two pyridomethene-BF_2 units in the molecules. The absorption spectra of **K6** and **K7** also displayed a blue-shifted in comparison to those of **K5** and **K4**, mainly caused by the large torsional angle (*e.g.*, 85°) between the phenyl and phenothiazine moieties (Fig. 4). When compared with **K6** and **K7**, dye **K8** displayed a further blue shift. The long wavelength absorption bands of **K6–K8** is assigned to an ICT transition mixed with π-π* character. Such an assignment is supported by the result of theoretical calculations, and is also evidenced by comparing the spectra of **K6–K8** with that of **P3**. It can be concluded that the incorporation of pyridomethene-BF_2 segments in all **K** dyes not only red-shifts the absorption edge, but also increases the molar extinction coefficient. As the maximal radiation energy of the sunlight appears at the wavelength 475 nm, it is anticipated that dyes **K1**-**K8** should possess an excellent light-harvesting ability in DSSC.

In order to understand the origins of the long wavelength absorption bands for dyes **K1**-**K8**, the absorption spectra of reference **P3** was measured for comparison. The long wavelength absorption bands of **K1**-**K8** were similar to the features reported for pyridomethene-BF_2 complex.[49] The long absorption band of **P3** (λ_{max} = 455 nm) overlaps well with those of **K1**-**K8**, and it also exhibits a high molar extinction coefficient (3.45×10^4 $M^{-1}cm^{-1}$) (Fig. 3b). In particular for **K6**-**K8**, the π-system of phenyl pyridomethene-BF_2 chromophore is nearly perpendicular to that of the phenothiazine. The spectral features of **K6**-**K8** are very close to that of **P3**, as a result of their high structural similarity.

The absorption spectra of dyes **K1**-**K8** and **R1**-**R2** on the surface of TiO_2 are shown in Fig. 5, and the corresponding data are collected in Table 1. When dyes **R1**-**R2** are absorbed onto the nanocrystalline TiO_2 particles (2 μm), the ICT absorption bands are blue-shifted by 17 and 44 nm, from 450 and 437 nm in THF solution to 433 and 394 nm, respectively. The ICT absorption maxima for dyes **K1**-**K8** on TiO_2 particles are close to those in THF solution. In general, when sensitizers were absorbed onto TiO_2 surface, a spectral shift may be induced by deprotonation and aggregation. The blue shift for dyes **R1** and **R2** is likely a result of deprotonation that weakens the electron-withdrawing ability of the carboxylate.[50] The effect of deprotonation was examined by the addition of triethylamine (TEA), which neutralizes the carboxylic acid in THF solution. The absorption spectra of the **K** and **R** dyes in the presence and absence of TEA are shown in Figs. 6 and S2. In an excessive amount of TEA, the ICT band of **R** exhibited an apparent blue shift, similar to that on the TiO_2 surface. However, the ICT band of **K** dyes did not change much in the presence of TEA. The existence of pyridomethene-BF_2 moieties in **K** dyes minimizes the influence by the carboxylate.

Electrochemical properties

Cyclic voltammetry (CV) was employed to evaluate the redox potentials of the dyes. All dyes **K1**-**K8** displayed two quasi-reversible oxidative waves (Figs. 7 and S3). The redox parameters are displayed in Table 1, and the HOMO-LUMO gaps are plotted in Fig. 8. The first oxidation potentials of dyes **K1**-**K8** are close to that of **R2**, and it responses to the removal of an electron from the phenothiazine moiety. A slightly lower oxidation potential of **K2** was observed due to the presence of an additional thiophene group adjacent to the cyanoacrylic acid.[7] For **R1**, the second oxidation potential is originated from the triarylamine moiety owing to its weaker electron-releasing ability than phenothiazine.[51-53] The second oxidation of dyes **K1**-**K8** occurred upon the removal of an electron from the pyridomethene-BF_2 complex and it is consistent with the oxidation potential of **P3**. The HOMO levels of all dyes were more positive than the reducing potential of iodine/iodide (0.4 V vs. the normal hydrogen electrode, NHE) pair, ensuring

Table 1 Photophysical and electrochemical data for **K**, **R** dyes and parent compound **P3**

Compd	λ_{abs}[a](nm)	λ_{max} ($\varepsilon \times 10^{-4}$, $dm^3\ mol^{-1}\ cm^{-1}$)[b]	λ_{abs}[c](nm) on TiO_2	$E_{0\text{-}0}$[d] (nm)/(eV)	E_{ox}[e]/V	E_{LUMO}[f]/V
K1	466	4.63	466	508 (2.44)	1.01	-1.43
K2	466	5.74	465	510 (2.43)	0.92	-1.51
K3	481	8.61	478	515 (2.41)	1.00	-1.41
K4	465	7.54	466	512 (2.42)	1.00	-1.42
K5	475	8.21	472	513 (2.42)	1.02	-1.40
K6	460	13.86	463	494 (2.51)	1.02	-1.49
K7	460	12.11	459	500 (2.48)	1.02	-1.46
K8	458	4.92	458	498 (2.49)	1.01	-1.48
R1	450	1.64	433	517 (2.40)	1.00	-1.40
R2	437	1.51	393	506 (2.45)	1.06	-1.39
P3	455	3.45	—	465 (2.67)	1.40	-1.27

[a] Maximum of the absorption band in THF. [b] Extinction coefficient of the absorption band in THF. [c] The maximum of the absorption band on 2 μm TiO_2 films. [d] Obtained from the intersection of normalized absorption and fluorescence spectra. [e] Oxidation potential measured vs Fc^+/Fc in THF were converted to normal hydrogen electrode (NHE) by addition of +0.63 V. [f] Energy of the LUMO of dyes estimated by $E_{ox} - E_{0\text{-}0}$.

sufficient driving force for the oxidized dyes to recapture an electron from the electrolyte. The LUMO levels of the dyes were deduced from the first oxidation potential and the 0-0 transition energy ($E_{0\text{-}0}$) estimated at the intersection of normalized absorption and fluorescence spectra. The LUMO levels of all the dyes was higher than the TiO_2 conductive band (–0.5 V), thus warranted the feasibility of electron injection.

Computational investigation

The effect of pyridomethene-BF_2 on photovoltaic performance of dyes **K1**-**K8** and **R1**-**R2** was further analysed by using DFT and time-dependent DFT calculations (TDDFT).[54-56] The electron distributions of frontier molecular orbitals are shown in Figs. 9 and S4-S5. A comparison with the results using Hartree-Fock (HF) and time-dependent HF with 6-31G (d,p) basis set is also included in Fig. S6. The optimized geometry of phenothiazine shows a tilted butterfly conformation (Fig. 4). The electron density of HOMO orbital is delocalized across both the phenothiazine and the pyridomethene-BF_2 moieties for dyes **K1**-**K7**. However, due to the large dihedral distortion of the phenyl pyridomethene-BF_2 substituent at the *N* (10) position of **K6**–**K8**, orbital overlap between the substituent and the main chromophore is prohibited. In addition, a nearly orthogonal conformation between the phenyl pyridomethene-BF_2 unit and phenothiazine is expected to widen the intermolecular distance on the surface of TiO_2, which is beneficial to the surface morphology. The electron distribution in the LUMO of all dyes is localized on the cyanoacrylic acid group. Electronic transitions with oscillator strength (*f*) larger than 0.1 are summarized in Table S1 (cf. Tables S2 for B3PW91/6-31G (d,p) and S3 for HF/6-31G (d,p)). The lowest energy absorption bands (S1 transition) for dyes **K1**-**K8** (*f* = 0.31～0.70) correspond to the HOMO→LUMO transition. The values are larger than that of the reference dyes **R1** (*f* = 0.27) and **R2** (*f* =0.26). The calculated results indicated that the long wavelength absorptions above 450 nm, mainly deriving from HOMO → LUMO transitions, are regarded as the ICT bands. It is found that dye **K3** displays the largest *f* values (0.70) of S1 transition due to its undisturbed π-conjugation. A relatively lower *f* value (0.31) of ICT transition for dye **K8** can be ascribed to the interruption of electronic coupling between the phenyl pyridomethene-BF_2 moiety and phenothiazine unit. The *f* values of dyes **K6** and **K7** are modest, yet their molar absorptivity was quite large in the spectra (Fig. 3b and Table 1). It can be attributed to the presence of two pyridomethene-BF_2

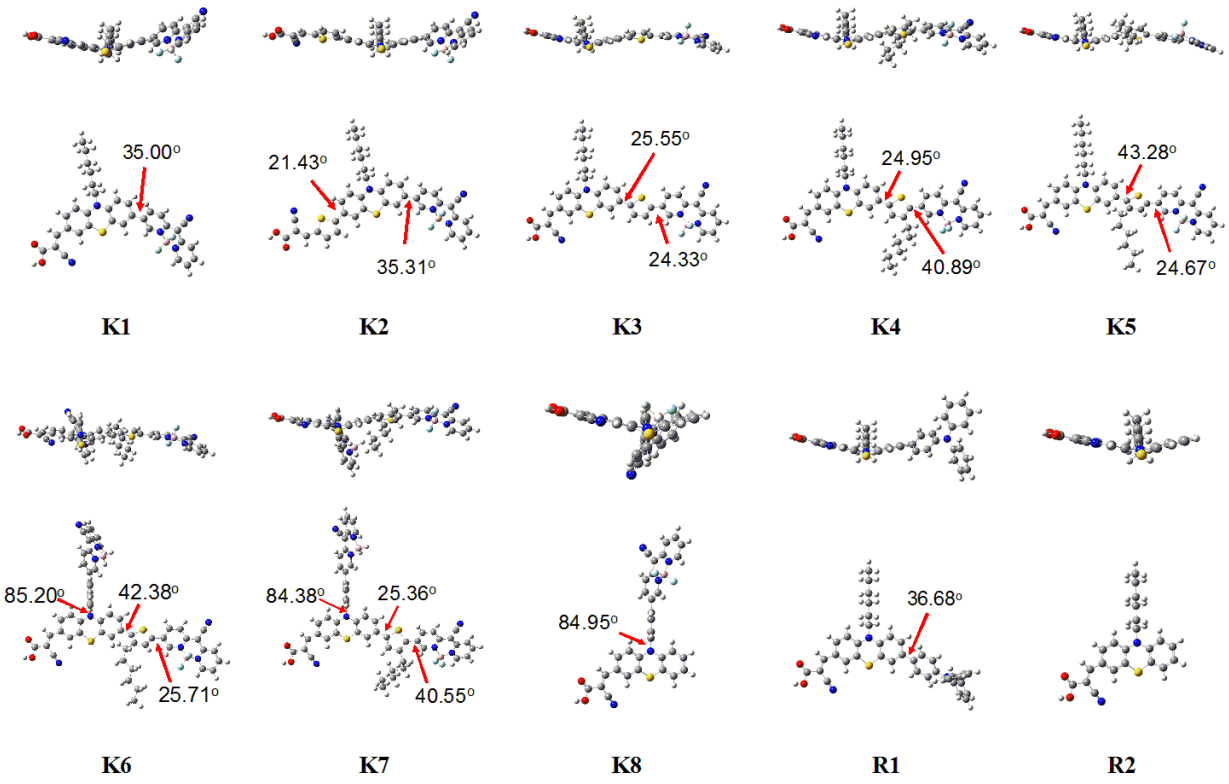

Fig. 4 The optimized structure of **K** and **R** dyes calculated with DFT on B3LYP-6-31G (d,p).

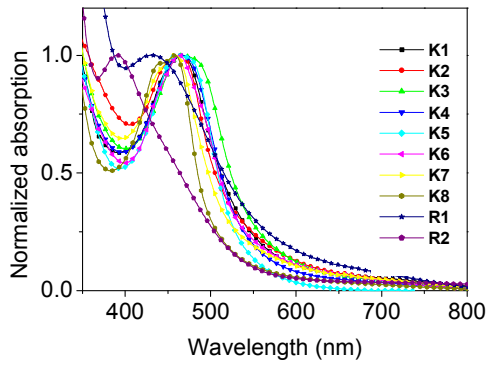

Fig. 5 Absorption spectra of **K** and **R** dyes on the TiO_2 films.

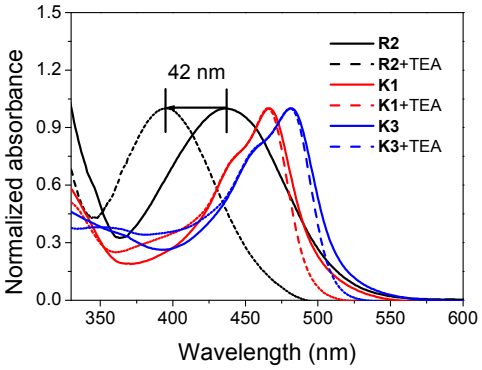

Fig. 6 Absorption spectra of dye **K1**, **K3** and **R2** in THF solutions before and after the addition of TEA.

units in the molecules. For example, a much higher intensity (*f* = 0.72) of HOMO-1→LUMO+1 transition (*i.e.*, π-π* transition of phenyl pyridomethene-BF_2 complex side chain) of **K6** is anticipated. The computed results comply well with the observed spectra of the dyes. The stimulated gas-phase absorption spectra of **K** and **R** dyes were shown in Fig. S7-S9.

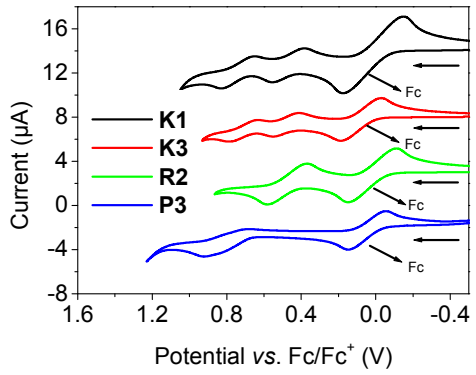

Fig. 7 Cyclic voltammograms of the dyes **K1**, **K3**, **R2** and **P3** recorded in THF solutions.

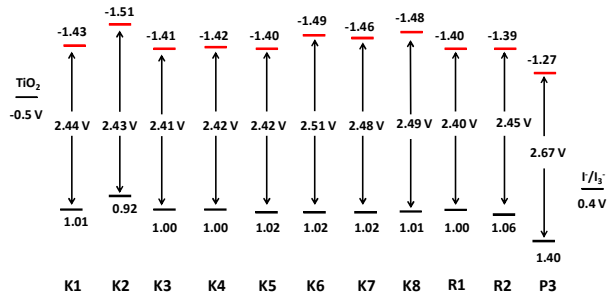

Fig.8 Scheme diagram of energy levels of TiO_2 conduction band, dyes and I^-/I_3^- redox couple.

Photovoltaic performance of DSSC

The DSSC based on the **K** and **R** dyes were fabricated by coating them on the surface of TiO_2 as sensitizers. The incident photo-to-current conversion efficiencies (IPCE) and *J*-*V* curves of all dyes are displayed under simulated AM 1.5 solar irradiation (100 mW · cm^{-2}) in Figs. 10 and 11, along with that of **R** dyes for comparison (10 μm transparent+5 μm scattering). Experiments by co-absorption with deoxycholic acid (DCA) were also carried out. The open-circuit photovoltage (V_{oc}), short-circuit photocurrent density (J_{sc}), fill factor (FF), and solar-to-electrical energy conversion efficiencies (η) are summarized in Table 2, where **N719** was used as a reference dye.

The IPCE values of most dyes are approximately 60% in the range of 400—550 nm, whereas that of **K3** exceeds 70% in the range of 480—560 nm. The IPCE spectrum for DSSC based on **K4** is the broadest among all **K** dyes. The overall quantum cell efficiency felt in the range of 3.82-5.15%. Among them the device made with **K8** exhibits the highest efficiency of 5.15% (J_{sc} = 12.64 mA cm^{-2}, V_{oc} = 0.65 V, FF = 0.63). In dye **K8**, a phenyl pyridomethene-BF_2 moiety was introduced on the phenothiazine nitrogen atom, unlike all the other dyes that were substituted at the 7th position. We speculated that the cell performance of all the **K** dyes was depressed to various degrees by the existence of π-π stacking that exists among pyridomethene-BF_2 moieties. It has been observed in previous studies that pyridomethene-BF_2 complex derivatives tend to form *J*-aggregations readily,[49] which lead to the quenching of charge separated species and the reduction of electron injection efficiency.[57,58] A typical example is shown by comparing the loading amounts of **K1** (4.08×10^{-7} mol cm^{-2}) and **R2** (3.75×10^{-7} mol cm^{-2}). Although the molecular size of **K1** is larger than that of **R2** by the presence of an extra pyridomethene-BF_2 group, the loading amount of the former was still higher than the latter.

A comparison between the two isomeric pairs of **K4**/**K5** and **K6**/**K7** is noteworthy. According to the IPCE spectra, dyes **K4** and **K7** performed better than their corresponding isomers **K5** and **K6**. The introduction of a hexyl chain on the thiophene unit helps the dyes to form a better surface morphology. Nevertheless, the position of the hexyl substituent on the thiophene unit exhibits a crucial influence on the photovoltaic performance. If the hexyl chain on the thiophene is attached away from the phenothiazine, like that of **K4** and **K7**, a better planarity (ca. 25°) is maintained between the two adjacent aromatic rings (Fig. 4). It leads to a better delocalization across the main chromophore from thiophene to the cyanoacrylate acceptor. On the contrary, when the hexyl chain is attached next to the phenothiazine, like that of **K5** and **K6**, a substantially larger dihedral angle (ca. 43°) appears between the thiophene and the phenothiazine. The conjugation of the main chromophore is interrupted, and results in a slow charge injection and small values of J_{sc}. Although dye **K6**, which contains two units of pyridomethene-BF_2 complex, exhibits the largest molar extinction coefficient, yet the device made with it displays the lowest J_{sc} value.

The charge injection efficiency is directly related to the IPCE value. The low IPCE for **K5** and **K6** can be further exemplified by an analysis of DFT and TDDFT calculations (Fig. 9 and Table S1). Upon photo-excitation, most electronic transitions in **K5** and **K6** proceed from HOMO or HOMO-1 to the LUMO+1 orbitals (i.*e.*, localized on the pyridomethene-BF_2 group) instead of to the LUMO orbital (localized on the cyanoacrylate moiety). This situation is opposite to the excitation processes in **K4** and **K7**. For instance, the HOMO-1 to

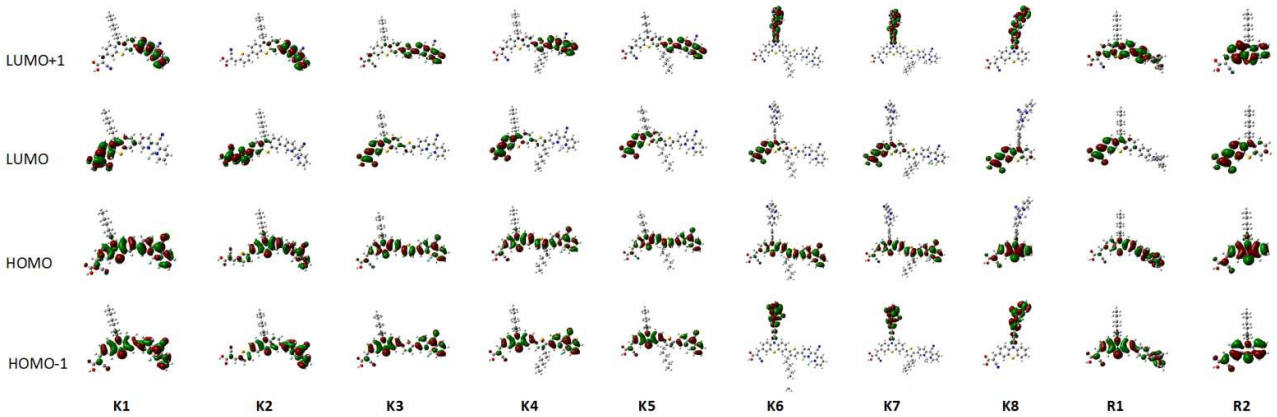

Fig. 9 Frontier orbitals of the **K** and **R** dyes optimized with DFT at the B3LYP/6-31G(d,p) level.

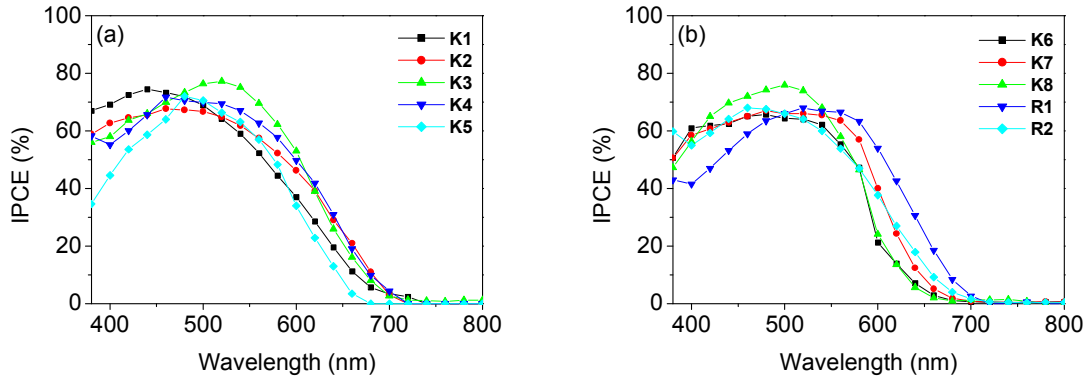

Fig. 10 The IPCE plots of DSSC made with (a) dyes **K1**–**K5** and (b) dyes **K6**–**K8** and **R** without DCA. TiO_2 film consisted of a 10 µm transparent layer and 5 µm scattering layer.

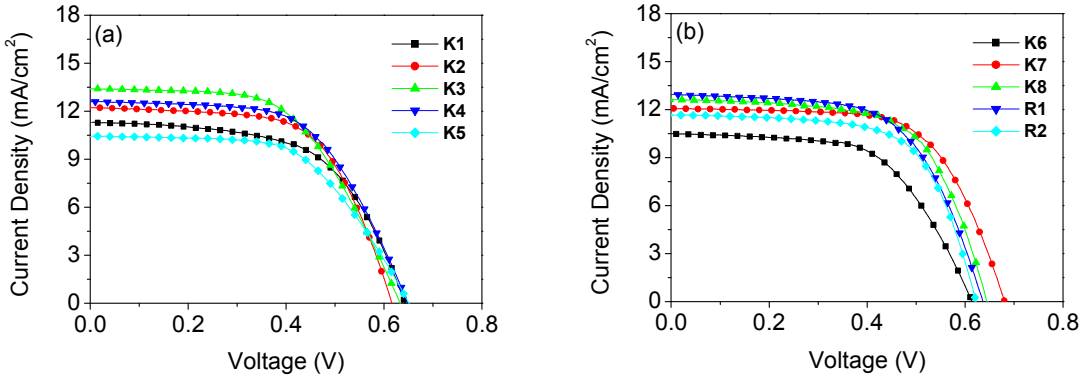

Fig. 11 Current-voltage plots for the DSSC made with (a) dyes **K1**–**K5** and (b) dyes **K6**–**K8** and **R** without DCA. TiO_2 film consisted of a 10 µm transparent layer and 5 µm scattering layer.

Table 2 DSSC performance parameters of **K** and **R** dyes with (10 mM) and without DCA[a]

dye	Amount[b]/molcm^{-2}	V_{oc}/V	J_{sc}/mA cm^{-2}	FF	η(%)
N719	1.88×10^{-7}	0.70	16.31	0.63	7.09
K1	4.08×10^{-7}	0.65	11.31	0.58	4.25
K1/DCA	1.66×10^{-7}	0.69	14.05	0.63	6.02
K2	3.52×10^{-7}	0.62	12.22	0.62	4.69
K2/DCA	3.01×10^{-7}	0.63	12.58	0.61	4.81
K3	6.50×10^{-7}	0.64	13.40	0.56	4.78
K3/DCA	1.49×10^{-7}	0.69	15.43	0.62	6.58
K4	2.05×10^{-7}	0.65	12.60	0.59	4.82
K4/DCA	0.80×10^{-7}	0.72	14.57	0.58	6.10
K5	1.91×10^{-7}	0.66	10.44	0.58	3.95
K5/DCA	0.66×10^{-7}	0.70	14.06	0.58	5.74
K6	3.25×10^{-7}	0.62	9.84	0.63	3.82
K6/DCA	2.34×10^{-7}	0.63	9.76	0.59	3.60
K7	2.98×10^{-7}	0.65	12.72	0.62	5.10
K7/DCA	2.49×10^{-7}	0.68	11.67	0.62	4.91
K8	5.01×10^{-7}	0.65	12.64	0.63	5.15
K8/DCA	4.23×10^{-7}	0.66	12.15	0.64	5.12
R1	2.15×10^{-7}	0.64	12.96	0.61	5.02
R1/DCA	1.93×10^{-7}	0.65	13.17	0.61	5.18
R2	3.75×10^{-7}	0.63	11.67	0.65	4.75
R2/DCA	2.70×10^{-7}	0.65	11.56	0.67	4.97

[a] Experiments were conducted with TiO_2 photoelectrodes with 10 μm transparent and 5 μm scattering thickness and 0.25 cm^2 working area on the FTO (8Ω/sq.) substrates. [b] Amount of dye adsorbed on TiO_2 film.

LUMO+1 transition of **K6** expresses a large oscillator strength (f = 0.72), comparing to the relatively smaller value (f = 0.49) of its HOMO to LUMO transition. Because the pyridomethene-BF_2 moiety is located on the opposite side of the TiO_2 surface, such a transition does not parallel to the formal direction of electron flow.

In order to further understand the behavior of the **K** and **R** dyes on the TiO_2 surface, the function of co-absorbent was investigated. DCA has been proven to suppress dye aggregation and effectively improve solar cell performances.[59] Photovoltaic data based on **K** and **R** dyes with 10 mM DCA at the given 10 μm thick TiO_2 film are summarized in Table 2. For all dyes, the V_{oc} values of DSSC in the presence of DCA were increased because of effective suppression of the dark current. As expected, dyes **K1**-**K5** are effective in increasing the photovoltaic parameters with DCA from 3.95～4.82% to 4.81～6.58%. The remarkable enhancement of power conversion

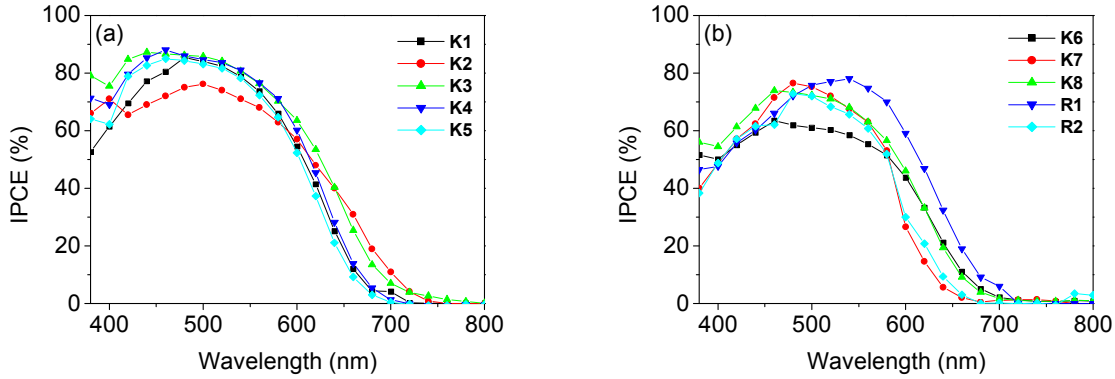

Fig. 12 The IPCE plots of DSSC made with (a) dyes **K1–K5** and (b) dyes **K6–K8** and **R** with DCA. TiO_2 film consisted of a 10 µm transparent layer and 5 µm scattering layer.

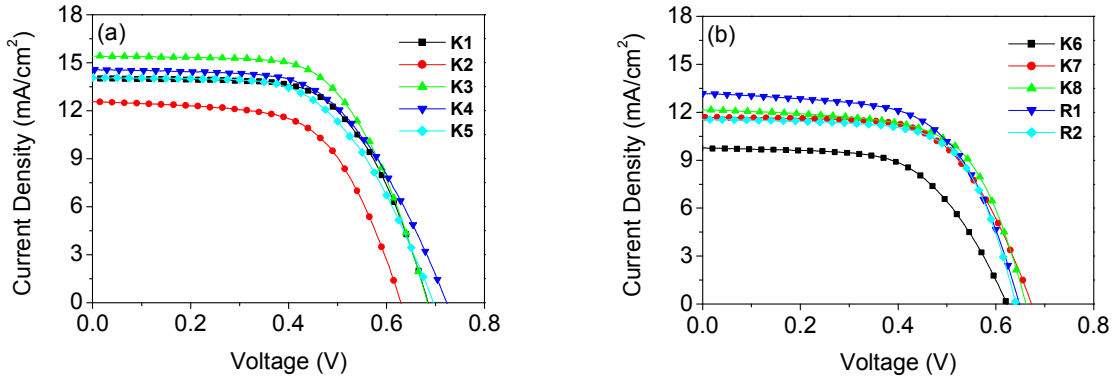

Fig. 13 Current-voltage plots for the DSSC made with (a) dyes **K1–K5** and (b) dyes **K6–K8** and **R** with DCA. TiO_2 film consisted of a 10 µm transparent layer and 5 µm scattering layer.

efficiency is ascribed mostly to the break-up of dye aggregation. The enhancement of J_{sc} values is shown in the IPCE spectra (Fig. 12). According to dye loading amount, **K1** and **K3**-**K5** show reduced dye loading amounts when DCA was added (Table 2). This result further confirms that a significant π-π interaction exists on the TiO_2 films of **K1** and **K3**-**K5** in the absence of DCA. A comparison between the isomer pair **K2** and **K3** reveals the significance of structural difference. Before adding DCA, the quantum efficiency of **K3** (η= 4.78%) is close to that of **K2** (η= 4.69%). After adding DCA, the quantum efficiency of **K3** (η = 6.58%) increased substantially, while that of **K2** (η = 4.81%) stays nearly the same. The two structures differ at the position of thiophenylene group. In **K2**, the thiophenylene group is located close to the cyanoacrylate anchoring site; therefore the structure is bent to an angular shape near to the TiO_2 surface. It is more difficult to readjust its surface alignment with the insertion of DCA.[7] A similar effect was observed on dyes **K6**-**K8** when each of them was co-adsorbed with 10 mM DCA. In the structure of dyes **K6**-**K8** there is a phenyl pyridomethene-BF_2 substituent at the *N*(10) position of phenothiazine, which causes the molecular shape more irregular than those of **K1**, **K4** and **K5**. Upon the addition of DCA, the alignment of the dyes was not much influenced by DCA. The cell performance of **K6**-**K8** reduced slightly as a result of reduced loading amounts. The improvement of cell performance was most pronounced in the case of **K3**, wherein the best efficiency of 6.58% was obtained, with a J_{sc} of 15.43 mA cm^{-2}, a V_{oc} of 0.69 V and an FF of 0.62. When compare with reference **R**, the overall conversion efficiency of dye **K1** (η = 6.02%) is higher than those of dyes **R1** (η = 5.18%) and **R2** (η = 4.97%) in an amount of ca. 16 and 21%, respectively, these results reveal an advantage of incorporating pyridomethene-BF_2 complex unit on **k** dyes skeleton to enhance the cell performance.

Further investigation on the effect on dye aggregation was performed by changing the dye film thickness. A thinner film of dye **K1** (5µm transparent+5 µm scattering) was prepared, and the cell made with it was compared with that made with a

thicker film (10 µm transparent+5 µm scattering). The photovoltaic parameters of IPCE and *J*-*V* curve are collected in Table S4 and Fig. S10. The DSSC cell made with thinner film of **K1** DSSC yielded a better performance of 5.15% (J_{sc} = 12.36 mA cm^{-2}, V_{oc} = 0.68 V, FF = 0.61) than that made with a thicker film (η= 4.25%). The dye loading amount for **K1** on 5 µm film is 2.28×10^{-7} mol cm^{-2}, which is about half of that on 10 µm film. After co-adsorbed with DCA (2 mM), the surface coverage for **K1** is slightly decreased (1.97×10^{-7} mol cm^{-2}), however, the power conversion efficiency of DSSC was increased to 5.66% (J_{sc} = 13.37 mA cm^{-2}, V_{oc} = 0.68 V, FF = 0.62). These results confirm again that breaking-up aggregation in the dyes containing pyridomethene-BF_2 moieties (*e.g.*, **K1** and **K3** to **K5**) is an effective way to improve the photovoltaic performance.

To get a deeper understanding on the interfacial charge transfer processes in DSSC, electrochemical impedance spectral (EIS) analysis were performed on the devices of **K** and **R** dyes co-adsorbed with DCA. The Nyquist and Bode plots of the DSSC are measured under a forward bias in the dark, and the results are shown in Fig. S11. In the Nyquist plots, the larger semicircles at lower frequencies indicate charge recombination resistance at the TiO_2/dye/electrolyte interface. The radius of the larger semicircle decreased in the order of **K4**>**K5**>**K3**～**K1**>**K7**>**K8**>**R1**～**R2**>**K2**～**K6**, indicating that the charge recombination resistance is roughly consistent with the values of V_{oc}. The additional long alkyl chain In **K4** and **K5** improves the dye layer morphology on TiO_2 and inhibits charge recombination. In Bode plots, the peaks at lower frequencies correspond to higher charge recombination rate, and are inversely proportional to the electron lifetime.[60,61] The peak maxima at lower-frequency range decreased in the order of **K4**>**K5**>**K3**～**K1**>**K7**>**K8**>**R1**～**R2**>**K2**～**K6**. The longer electron lifetime of **K4** and **K5** implies that by the introduction of two long alkyl chains the charge recombination rate across the TiO_2/dye/electrolyte interface can be effectively inhibited.

Stability of the sensitizers

The stability of dyes is an important factor for a sustained operation on practical applications of DSSC. Dyes adsorbed on 10 µm nanocrystalline TiO_2 films were continuously irradiated by AM 1.5 light without redox mediators according to Katoh's method.[62] After 30 min the absorbance of reference dyes **R1** and **R2** decreased to some extent, the spectra of **K** dyes stayed nearly invariant both in absorption intensity and band shape

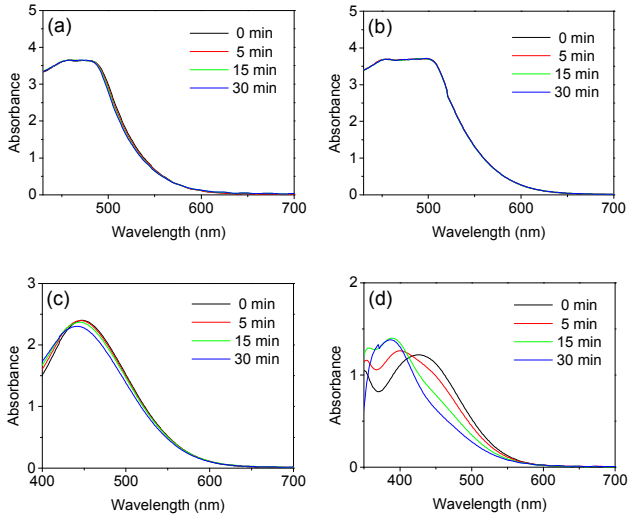

Fig. 14 Absorption spectra of (a) **K1**, (b) **K4**, (c) **R1**, and (d) **R2** absorbed on nanocrystalline TiO_2 films before and after light irradiation (30 min).

(Figs 14 and S12). It indicates a high photo-stability of the dyes, and assures their good practical value.

Summary

In summary, a series of metal-free organic dipole dyes containing phenothiazine and pyridomethene-BF_2 moieties were synthesized, and their usage on DSSC was investigated. Taking advantage the high molar absorptivity of pyridomethene-BF_2 group, these dyes displayed remarkable light harvesting efficiency. With the assistance of co-absorption of DCA, the best solar cell performance of dye **K3** reaches to a high quantum efficiency 6.58%, with J_{sc} 15.43 mA cm^{-2}, V_{oc} 0.69 V, and FF 0.62.

There are a few unique structural features that influence the cell performance, are noteworthy. The relative position of a thiophenylene group in **K2** and **K3** makes a significant difference on their quantum efficiency. In the absence of DCA, the two isomers performed comparably (4.69% and 4.78%, respectively). In the presence of DCA, however, the quantum efficiency of **K3** increased to almost 40% (up to 6.58%), while that of **K2** stayed the same (4.81%). The position of thiophenylene group in **K2** caused the molecules to bend in a larger angle near the surface of TiO_2, therefore became less sensitive to the influence of DCA.

The long hexyl substituents in **K1**-**K7** have an effect of covering the surface of TiO_2 and improving the film morphology. The relative position of the second hexyl group on the thiophene moieties of isomeric pairs of **K4**/**K5** and **K6**/**K7** induced an apparent difference on cell performance. In cases where the hexyl group is located close to the phenothiazine, like that in **K5** and **K6**, the J_{SC} values (10.44 and 9.84 mA cm^{-2}) were smaller than those in **K4** and **K7** (12.60 and 12.72 mA cm^{-2}). It is caused by the twisting of dihedral angles

between adjacent aryl groups due to the steric hindrance of the hexyl group.

The addition of second pyridomethene-BF_2 groups in **K6** and **K7** increased the absorption intensity substantially, so that more photons can be harvested by these dyes. Both the J_{SC} (12.72 mA cm^{-2}) and η (5.10%) values of **K7** are among the highest before adding DCA. However, the presence of two pyridomethene-BF_2 groups increased the size of the dye molecules, and reduced their sensitivity toward DCA. Upon adding DCA, the dyes with long rod-shaped geometry, like those of **K1** and **K3**-**K5**, can be benefited to a higher degree than **K6** and **K7**.

With respect to the reference **R** dyes, the incorporation of pyridomethene-BF_2 unit can indeed increase the molar extinction coefficient, which is in favour of light harvesting. The effect of pyridomethene-BF_2 group on the absorption spectra and charge transition characteristics was analyzed with the aid of DFT and time-dependent DFT theoretical models. Furthermore, the introduction of the pyridomethene-BF_2 complex unit in **K** dyes show an excellent photo-stability as compared with **R** dyes.

Experimental section

Characterization

^1H, ^{13}C and ^{19}F NMR spectra were recorded on a Bruker 400 and 500 MHz spectrometer. Fast atom bombardment (FAB) and time-of flight (TOF) mass spectra were recorded on a Jeol JMS 700 double-focusing spectrometer. UV spectra were measured on a Jasco V-530 double beam spectrophotometer. Fluorescence spectra were recorded on a Hitachi F-4500 fluorescence spectrophotometer. Cyclic voltammogram were performed with a CHI-621A electrochemical analyzer. All measurements were carried out at room temperature with a conventional three electrode configuration that consisted of a platinum working electrode, an auxiliary electrode, and a nonaqueous $Ag/AgNO_3$ reference electrode.

Materials and Reagents

Tetra-*n*-butylammonium hexafluorophosphate ($TBAPF_6$), 4-tert-butylpyridine (4-TBP), lithium iodide, and 2-cyanoacetic acid were purchased from Fluka. All other solvents and chemicals were purchased from Aldrich. The Thin-layer chromatography (TLC) was conducted with Merck KGaA precoated TLC Silica gel 60F254 aluminum sheets. Flash column chromatography was performed on glass columns packed with silica gel using Silicycle UltraPure SilicaFlash P60, 40–63 mm (230–400 mesh). Unless otherwise specified, all reactions and manipulations were carried out under a nitrogen atmosphere, and the purity of all commercial materials and solvents were more than 98%. Solvents of reagent grade were used for syntheses and those of spectroscopy grade for spectra measurements. Solvents were dried by standard procedures. The dye bis(tetrabutylammonium)-cis-di(thiocyanato)-N,N'-bis(4-carboxylato-4'-carboxylic acid-2,2'-bipyridine)ruthenium (coded as **N719**) and TiO_2 paste were purchased from Solaronix S. A., Switzerland. The characterization data for the compounds **K**, **R1** and **P3** are provided in the Supporting Information. Typical synthetic procedures are as follows:

General procedures for Suzuki reaction

A heterogeneous mixture of 2M K_2CO_3 (aq) (2.2 mL), THF (3.00 mL), pinacol ester derivatives (1.05 mmol), $Pd(PPh_3)_4$ (2 mol %), and aryl bromide (1.00 mmol) were heated at 80 °C under an argon atmosphere for 18 h. After cooling, the reaction was extracted with CH_2Cl_2. The organic layer was dried over anhydrous $MgSO_4$. The filtrate was concentrated under reduced pressure. Further purification was performed by column chromatograph.

General procedures for Knoevenagel condensation reaction

A mixture of aldehyde precursor (1.10 mmol), cyanoacetic acid (1.30 mmol), and ammonium acetate (0.28 mmol) in acetic acid (20 mL) was placed in a three-necked flask under a nitrogen atmosphere and was stirred at 80 °C for 18 h. After cooling, the reaction was extracted with CH_2Cl_2. The organic layer was dried over anhydrous $MgSO_4$. Further purification was performed by column chromatograph.

Computation method

Computations were performed using the Gaussian 03 program package. The geometry was optimized by using B3LYP (Becke three parameters hybrid functional with Lee-Yang-Parr correlation functionals) with the Pople 6-31G(d,p) atomic basis set.[54-56]

Device fabrication

The TiO_2 films used were comprised of a transparent layer and a scattering layer with thickness of 5 or 10 and 4 mm, respectively, as measured by a profilometer (Dektak3, Veeco/Sloan InstrumentsInc., USA). The TiO_2 electrodes with a 0.25 cm^2 geometric area were immersed in the THF solution containing $3x10^{-4}$ M organic sensitizers or in an acetonitrile/tert-butanol (1:1 by vol.) containing $3x10^{-4}$ M N719 [cis-di(thiocyanato)bis(2,2'-bipyridyl-4,4'-dicarboxylato)-ruthenium(II) bis(tetrabutylammonium)] for 12 h, then rinsed with anhydrous acetonitrile and dried. The best performance of DSSC with deoxycholic acid (DCA) as the co-adsorbent was found to have the concentration of DCA at 10 mM. Another piece of FTO with sputtering 100 nm thick Pt was used as a counter electrode. The active area was controlled at a dimension of 0.25 cm^2 by adhering 60 μm thick polyester tape on the Pt electrode. The photocathode was placed on top of the counter electrode and was tightly clipped together to form a cell. Electrolyte was then injected into the seam between two electrodes. An acetonitrile solution containing LiI (0.5 M), I_2 (0.05 M), and 4-tert-butylpyridine (0.5 M) was used as the

electrolyte. Devices made of a commercial dye **N719** under the same condition was compared as a reference.

Photovoltaic Performance Measurements

Photocurrent–voltage characteristics of the DSSC were recorded with a potentiostat/galvanostat (CHI650B, CH Instruments, Inc.,USA) at a light intensity of 1.0 sun calibrated by an Oriel reference solar cell (Oriel 91150, Newport Corp.). Incident photo-to-current conversion efficiency (IPCE) curves were obtained at short-circuit condition. The light source was a class A quality solar simulator (PEC-L11, AM 1.5G, Peccell Technologies, Inc.); light was focused through a monochromator (Oriel Instrument, model 74100) onto the photovoltaic cell and measured with an optical detector (Oriel Instrument, model 71580) and power meter (Oriel Instrument, model 70310). Electrochemical impedance spectra were recorded for DSSC at an open-circuit voltage (V_{oc}) in the dark at -0.55 V at room temperature. The frequencies explored ranged from 10 mHz to 100 kHz.

Acknowledgements

Financial supports from the National Science Council of Taiwan and Academia Sinica are gratefully acknowledged.

Notes and references

1 B. O'Regan and M. Grätzel, *Nature*, 1991, **353**, 737.
2 M. Grätzel, *J. Photochem. Photobiol., A*, 2004, **164**, 3.
3 M. K. Nazeeruddin, A. Kay, L. Rodicio, R. Humphry-Baker,E. Műller, P. Liska, N. Vlachopoulos and M. Grätzel, *J. Am.Chem. Soc*., 1993, **115**, 6382.
4 M. K. Nazeeruddin, P. Pechy, T. Renouard, S. M. Zakeeruddin,R. Humphry-Baker, P. Comte, P. Liska, L. Cevey, E. Costa,V. Shklover, L. Spiccia, G. B. Deacon, C. A. Bignozzi and M. Grätzel, *J. Am. Chem. Soc*., 2001, **123**, 1613.
5 A. Yella, H. W. Lee, H. N. Tsao, C. Yi, A. K. Chandiran, M. K. Nazeeruddin, E. W. G. Diau, C. Y. Yeh, S. M. Zakeeruddin and M. Grätzel, *Science*, 2011, **334**, 629.
6 Z.-S. Wang, Y. Cui, K. Hara, Y. Dan-oh, C. Kasada and A. Shinpo, *Adv. Mater*., 2007, **19**, 1138.
7 C.-J. Yang, Y. J. Chang, M. Watanabe, Y.-S. Hon and T. J. Chow, *J. Mater. Chem.*, 2012, **22**, 4040.
8 Y. J. Chang, P.-T Chou, Y.-Z. Lin, M. Watanaba, C.-J. Yang, T.-M Chin, T. J. Chow, *J. Mater. Chem*., 2012, **22**, 21704.
9 Y. Hua, S. Chang, J. He, C. Zhang, J. Zhao, T. Chen, W.-Y. Wong, W.-K, Wong, X. Zhu. *Chem. Eur. J*. 2014, **20**, 6300.
10 Y. Hua, S. Chang, D. Huang, X. Zhou, X. Zhu, J. Zhao, T. Chen, W.-Y. Wong and W.-K, Wong, Chem. Mater. 2013, **25**, 2146
11 A. Ehret, L. Stuhl and M. T. Spitler, *J. Phys. Chem. B*, 2001, **105**, 9960.
12 S. Ito, S. M. Zakeeruddin, R. Humphry-Baker, P. Liska,R. Charvet, P. Comte, M. K. Nazeeruddin, P. Péchy, M. Takata, H. Miura, S. Uchida and M. Grätzel, *Adv. Mater*., 2006, **18**, 1202.
13 H. Chen, H. Hung, X, Hung, J. N. Clifford, A. Forneli, E, Palomares, X, Zheng, L, Zheng, X, Wang, P, Shen, B, Zhao and S, Tan, *J. Phys. Chem. C*, 2010, **114**, 3280.
14 Y.-J. Chang and T. J. Chow, *Tetrahedron*, 2009, **65**, 4726.
15 Y.-J. Chang and T. J. Chow, *Tetrahedron*, 2009, **65**, 9626.
16 Y. J. Chang and T. J. Chow, *J. Mater. Chem*., 2011, **21**, 9523.
17 Y.-J. Chang M. Watanaba P.-T. Chou and T. J. Chow *Chem. Commun*., 2012, **48**, 726.
18 Y.-D. Lin, C.-T. Chien, S.-Y. Lin, H.-H. Chang, C.-Y. Liu, T. J. Chow, *J. Photochem. Photobiol. A* 2011, **222**, 192.
19 Y.-D. Lin and T. J. Chow, *J. Photochem. Photobiol. A* 2012, **230**, 47.
20 Y.-D. Lin and T. J. Chow, *J. Mater. Chem*., 2011, **21**, 14907.
21 Z. Ning and H. Tian, *Chem. Commun*., 2009, 5483.
22 Z. Ning, Q. Zhang, W. Wu, H. Pei, B. Liu and H. Tian, *J. Org. Chem*., 2008, **73**, 3791.
23 D. P. Hagberg, J.-H. Yum, H. Lee, F. D. Angelis, T. Marinado, K. M. Karlsson, R. Humphry-Baker, L. Sun, A. Hagfeldt, M. Grätzel and M. K. Nazeeruddin, *J. Am. Chem. Soc*., 2008, **130**, 6259.
24 L.-L. Tan, J.-F. Huang, Y. Shen, L.-M. Xiao, J.-M. Liu, D.-B. Kuang and C.-Y. Su, *J. Mater. Chem. A*, 2014, **2**, 8988.
25 A. Loudet and K. Burgess, *Chem. Rev*. 2007, **107**, 4891.
26 C. Peters, A. Billich, M. Ghobrial, K. Högenauer, T. Ullrichand P. Nussbaumer, *J. Org. Chem*., 2007, **72**, 1842.
27 N. Boens, V. Leen and W. Dehaen, *Chem. Soc. Rev*., 2012, **41**,1130.
28 A. Kamkaew, S. H. Lim, H. B. Lee, L. V. Kiew, L. Y. Chungand K. Burgess, *Chem. Soc. Rev*., 2013, **42**, 77.
29 S. Hattori, K. Ohkubo, Y. Urano, H. Sunahara, T. Nagano,Y. Wada, N. V. Tkachenko, H. Lemmetyinen and S. Fukuzumi, *J. Phys. Chem. B*, 2005, **109**, 15368.
30 S. Erten-Ela, M. D. Yilmaz, B. Icli, Y. Dede, S. Icli andE. U. Akkaya, *Org. Lett*., 2008, **10**, 3299.
31 D. Kumaresan, R. P. Thummel, T. Bura, G. Ulrich and R. Ziessel, *Chem.–Eur. J*., 2009, **15**, 6335.
32 C. Y. Lee and J. T. Hupp, *Langmuir*, 2010, **26**, 3760.
33 S. Kolemen, Y. Cakmak,S. Erten-Ela, Y. Altay, J. Brendel, M. Thelakkat and E. U. Akkaya, *Org. Lett*., 2010, **12,** 3812.
34 S. Kolemen,O. A. Bozdemir, Y. Cakmak, G. Barin, S. Erten-Ela,M. Marszalek, J.-H. Yum, S. M. Zakeeruddin, M. K. Nazeeruddin, M. Grätzel and E. U. Akkaya, *Chem. Sci*., 2011, **2**, 949.
35 M. Mao, J.-B. Wang, Z.-F. Xiao, S.-Y. Dai and Q.-H. Song, *Dyes Pigm*., 2012, **94**, 224.
36 K. Gräf, T. Körzdörfer, S. Kümmel and M. Thelakkat, *New J. Chem*., 2013, **37**, 1417.
37 Y. Ooyama, Y. Hagiwara, T. Mizumo, Y. Harima and J. Ohshita, *New J. Chem*., 2013, **37**, 2479.
38 Y. Ooyama, Y. Hagiwara, T. Mizumo,Y. Harima and J. Ohshita, *RSC Adv*., 2013, **3**, 18099.
39 M. Mao, X.-L. Zhang, X.-Q. Fang, G.-H. Wu, S.-Y. Dai, Q.-H Song and X.-X. Zhang, J. Power Souces. 2014, **268**, 965.
40 M. Mao, X.-L. Zhang, X.-Q. Fang, G.-H. Wu, Y. Ding, X.-L. Liu, S.-Y. Dai and Q.-H Song, *Org. Electron*. 2014, **15**, 2079.
41 J.-F. Lefebvre, X.-Z. Sun, J. A. Calladine, M. W. George and E. A. Gibson, *Chem. Commun*., 2014, **50**, 5258.
42 S. P. Singh and T. Gayathri, *Eur. J. Org. Chem*. 2014, 4689.
43 Y. Kubo, D. Eguchi, A. Matsumoto, R. Nishiyabu, H. Yakushiji, K. Shigaki and M. Kaneko, *J. Mater. Chem*. *A* 2014, **2**, 5204.
44 Y. Mizuno, Y. Yisilamu, T. Yamaguchi, M. Tomura, T. Funaki, H. Sugihara and K. Ono, *Chem. Eur. J.* 2014, **20**, 13286.
45 Y.-D. Lin and T. J. Chow, *RSC Adv*., 2013, **3**, 17924.
46 Y. Wu, M. Marszalek, S. M. Zakeeruddin, Q. Zhang, H. Tian, M. Grätzel and W. Zhu, *Energy Environ. Sci*., 2012, **5**, 8261.
47 W. Li, Y. Wu, X. Li, Y. Xie and W. Zhu, *Energy Environ. Sci*., 2011, **4**, 1830.
48 M. Akhtaruzzaman, Y. Seya, N. Asao, A. Islam, E. Kwon, . El-Shafei, L. Han, Y. Yamamoto, *J. Mater. Chem*., 2012, **22**, 10771.
49 Y. Kubota, T. Tsuzuki, K. Funabiki, M. Ebihara and M. Matsui, *Org. Lett*., 2010, **12**, 4010.
50 H.-Y. Yang, Y.-S. Yen, Y.-C. Hsu, H.-H. Chou and J.T. Lin, *Org. Lett*., 2010, **12**, 16.

51 X. Q. Zhu, Z. Dai, A. Yu, S. A. Wu, J. P. Cheng, *J. Phys. Chem. B* 2008, **112**, 11694.
52 H. Tian, X. Yang, J. Cong, R. Chen, C. Teng, J. Liu, Y. Hao, L. Wang and L. Sun, *Dyes Pigm*., 2010, **84**, 62.
53 J.-H. Zhao, X. Yang, M. Cheng, S.-F. Li and L. Sun, *ACS Appl. Mater. Interfaces*, 2013, **5**, 5227.
54 M.J. Frisch, G.W. Trucks, H.B. Schlegel, G.E. Scuseria, M.A. Robb, J.R. Cheeseman, J.A. Montgomery Jr., T. Vreven, K.N. Kudin, J.C. Burant, J.M. Millam, S.S.Iyengar, J. Tomasi, V. Barone, B. Mennucci, M. Cossi, G. Scalmani, N. Rega, G.A. Petersson, H. Nakatsuji, M. Hada, M. Ehara, K. Toyota, R. Fukuda, J. Hasegawa, M. Ishida, T. Nakajima, Y. Honda, O. Kitao, H. Nakai, M. Klene, X. Li, J.E Knox, H.P. Hratchian, J.B. Cross, V. Bakken, C. Adamo, J. Jaramillo, R. Gomperts, R.E. Stratmann, O. Yazyev, A.J. Austin, R. Cammi, C. Pomelli, J.W. Ochterski, P.Y. Ayala, K.Morokuma, G.A. Voth, P. Salvador, J.J. Dannenberg, V.G. Zakrzewski, S. Dapprich, A.D. Daniels, M.C. Strain, O. Farkas, D.K. Malick, A.D. Rabuck, K. Raghavachari, J.B. Foresman, J.V. Ortiz, Q. Cui, A.G. Baboul, S. Clifford, J. Cioslowski, B.B. Stefanov, G. Liu, A. Liashenko, P. Piskorz, I. Komaromi, R.L. Martin, D.J. Fox, T. Keith, M.A. Al-Laham, C.Y. Peng, A. Nanayakkara, M. Challacombe, P.M.W. Gill, B. Johnson, W. Chen, M.W. Wong, C. Gonzalez, J.A. Pople, Gaussian 03, Gaussian Inc., Pittsburgh, PA, 2003.
55 A.D. Becke, *J. Chem. Phys*. 1993, **98**, 5648.
56 R. Ditchfield, W.J. Hehre, J.A. Pople, *J. Chem. Phys*. 1971, **54**, 724.
57 H. Choi, C. Baik, S. O. Kang, J. Ko, M. S. Kang, M. K. Nazeeruddin, M. Grätzel, *Angew. Chem*. 2008, **120**, 333.
58 Y. Ooyama, Y. Harima, *ChemPhysChem* 2012, **13**, 4032.
59 R. Chen, X. Yang, H. Tian, X. Wang, A. Hagfeldt and L. Sun, *Chem. Mater*., 2007, **19**, 4007.
60 M. Adachi, M. Sakamoto, J. Jiu, Y. Ogata, S. Isoda, *J. Phys. Chem. B* 2006, **110**, 13872.
61 Q. Wang, J. Moser, M. Grätzel, *J. Phys. Chem. B* 2005, **109**, 14945.
62 R. Katoh, A. Furube, S. Mori, M. Miyashita, K. Sunahara, N. Koumura and K. Hara, *Energy Environ. Sci.* 2009, **2**, 542.